NeuroImage 72 (2013) 227–236

Contents lists available at SciVerse ScienceDirect

NeuroImage

journal homepage: www.elsevier.com/locate/ynimg

EEG correlates of time-varying BOLD functional connectivity

Catie Chang [a,*], Zhongming Liu [a], Michael C. Chen [b], Xiao Liu [a], Jeff H. Duyn [a]

[a] Advanced MRI Section, Laboratory of Functional and Molecular Imaging, National Institute of Neurological Disorders and Stroke, National Institutes of Health, Bethesda, MD 20892, USA
[b] Department of Psychology, Stanford University, Stanford, CA 94305, USA

ARTICLE INFO

Article history:
Accepted 24 January 2013
Available online 31 January 2013

ABSTRACT

Recent resting-state fMRI studies have shown that the apparent functional connectivity (FC) between brain regions may undergo changes on time-scales of seconds to minutes, the basis and importance of which are largely unknown. Here, we examine the electrophysiological correlates of within-scan FC variations during a condition of eyes-closed rest. A sliding window analysis of simultaneous EEG–fMRI data was performed to examine whether temporal variations in coupling between three major networks (default mode; DMN, dorsal attention; DAN, and salience network; SN) are associated with temporal variations in mental state, as assessed from the amplitude of alpha and theta oscillations in the EEG. In our dataset, alpha power showed a significant inverse relationship with the strength of connectivity between DMN and DAN. In addition, alpha power covaried with the spatial extent of anticorrelation between DMN and DAN, with higher alpha power associated with larger anticorrelation extent. Results suggest an electrical signature of the time-varying FC between the DAN and DMN, potentially reflecting neural and state-dependent variations.

Published by Elsevier Inc.

Introduction

Network analysis of spontaneous blood oxygen level dependent (BOLD) signals has revealed a remarkable degree of organization, with spatial patterns of correlated time series that are quite reliably identified (Beckmann et al., 2005; Smith et al., 2009) and are interpreted to reflect functional connectivity between regions. Importantly, the correlation structure within and between networks has been observed to reconfigure across a range of conscious and unconscious states (e.g. (Horovitz et al., 2009; Samann et al., 2011; Vanhaudenhuyse et al., 2010) as well as on finer-grained temporal scales (seconds to minutes) within the duration of a typical resting state scan. For example, an anti-correlated relationship between two major intrinsic brain networks, the default-mode network (DMN) and dorsal attention network (DAN) (Fox et al., 2005; Greicius et al., 2003), appears to occur in occasional, transient epochs when non-stationary time series analysis is applied (Chang and Glover, 2010; Popa et al., 2009). Similar fluctuations in correlation patterns have been observed across other networks in humans with fMRI (Kiviniemi et al., 2011; Rack-Gomer and Liu, 2012; Sakoglu et al., 2010) and MEG (de Pasquale et al., 2010), and in the BOLD signal of anesthetized monkeys (Hutchison et al., 2012).

Since the brain is constantly active, the observation that functional connectivity varies over time during wakeful resting-state conditions is somewhat unsurprising. However, it is not clear to what degree the apparent connectivity modulation reflects neural phenomena such as conscious mental activity (Shirer et al., 2012), transient activation events (Petridou et al., 2012), or the inherent dynamics of a small-world network architecture (Honey et al., 2007; Sporns, 2011), and to what extent it is simply due to episodes of random synchrony (Handwerker et al., 2012) or time-varying levels of physiological noise (Birn et al., 2006; Chang and Glover, 2009; Glover et al., 2000; Shmueli et al., 2007) that may artificially couple and decouple fMRI signals across the course of a scan.

Here, we use simultaneous EEG–fMRI to examine potential electrophysiological correlates of time-varying BOLD functional connectivity during eyes-closed resting state. Resting-state EEG rhythms are themselves nonstationary, having ongoing fluctuations in amplitude and phase that track shifts in vigilance and cognitive state, and hence may be used as an independent variable with which to interrogate resting-state fMRI data (see (Laufs, 2008) for a review). The majority of resting-state EEG–fMRI studies to date have sought the electrophysiological signatures of resting-state network activity by regressing the power in one or more EEG frequency bands against BOLD signal time series (see (Laufs, 2008) for a review), after convolving the former with a canonical or derived hemodynamic response function (e.g. (de Munck et al., 2008; Goldman et al., 2002)). An alternative approach is to relate levels of EEG power to the *functional connectivity* within and between networks rather than to the BOLD signal activity itself. With an inter-subject analysis, Hlinka et al. determined that the functional connectivity within the DMN was related to individual differences in the mean levels of delta, alpha, and beta power (Hlinka et al., 2010). Lu et al. found that both delta power connectivity and BOLD functional connectivity between the left and right somatosensory cortex in the

* Corresponding author at: Advanced MRI Section/LFMI/NINDS, National Institutes of Health, 10 Center Dr., Rm. B1D723, Bethesda, MD 20892-1065, USA.
E-mail address: catie.chang@nih.gov (C. Chang).

1053-8119/$ – see front matter. Published by Elsevier Inc.
http://dx.doi.org/10.1016/j.neuroimage.2013.01.049

rat was modulated by anesthetic dose (Lu et al., 2007). Using a psycho-physiological interactions analysis, Scheeringa et al. report an association between within-scan increases in alpha power and decreases in BOLD connectivity within the visual cortex, as well as decreases in negative coupling between visual and default-mode regions (Scheeringa et al., 2012).

Along similar lines, the present study investigates potential EEG correlates of within-scan fluctuations in functional connectivity between three major RSNs (DMN, DAN, and salience network; SN) during eyes-closed resting state. Anti-correlated behavior has been found between nodes of the DMN and SN (Fransson, 2005; Uddin et al., 2009), in addition to those of the DMN and DAN; moreover, an interesting dynamic relationship between all three networks has been proposed, with the SN perhaps acting to coordinate switches in activity between DMN and DAN (Menon and Uddin, 2010). In our earlier study (Chang et al., 2010), nodes of the SN (e.g., anterior cingulate cortex and anterior insula) were found to be amongst regions having the highest variability of sliding-window functional connectivity with a key node of the DMN (posterior cingulate cortex), further motivating consideration of the SN in addition to DMN and DAN.

Using a sliding-window analysis of simultaneous EEG–fMRI data, we examine whether temporal variations in pairwise coupling between these three networks are associated with temporal variations in the amplitude of EEG power, focusing specifically on the alpha and theta frequency bands. Previous studies have established that the power in alpha and theta EEG oscillations is modulated as a function of vigilance; drowsiness and sleep onset are characterized by diminished alpha power and increased theta and delta power (reviewed in (Klimesch, 1999)), as are performance lapses in continuous tasks (Makeig and Inlow, 1993). We therefore regard the EEG alpha and theta spectral power as a state variable with which to query changes in BOLD functional connectivity. The work described in this article has been presented as a conference abstract (Chang et al., 2012).

Materials and methods

Data acquisition and pre-processing

Simultaneous EEG–fMRI data from 10 healthy adults (6 female, aged 33.3 ± 15.6 years) were included in this study. Seven of the participants (numbered as Subjects 1–6, 10 in the Results) were scanned at the National Institutes of Health and 3 were scanned at Stanford University (Subjects 7–9). A comparison of the main acquisition parameters is provided in Table 1, and described in detail below. All subjects provided written, informed consent and all protocols were approved by the Institutional Review Boards of the respective institutes.

Table 1
Summary of major acquisition parameters.

	NIH	Stanford
Subject #	1–6, 10	7–9
EEG		
System	BrainAmps, 32-channel cap	EGI, 256 channel cap
fMRI		
System	GE Signa, 3 Tesla 16-channel head coil	GE Discovery MR750, 3 Tesla 8-channel head coil
Pulse sequence	EPI, SENSE factor = 2	Spiral in-out
Voxel size	3.45×3.45 mm^2 in-plane, 4 mm slice thickness, 0 mm skip	3.45×3.45 mm^2 in-plane, 4 mm slice thickness, 0 mm skip
# slices	30	30
TR/TE	1.5 s/30 ms	2.04 s/30 ms
Scan duration	9.75 min	11.76 min (1 subject), 12.24 min (2 subjects)

Stanford dataset

Magnetic resonance imaging was performed on a 3T whole-body scanner (Discovery MR750, GE Healthcare Systems, Milwaukee, WI) with a GE 8-channel head coil. A gradient echo spiral-in/out pulse sequence (Glover and Law, 2001) was used for functional imaging (TR = 2040 ms, TE = 30 ms, flip angle = 77°, matrix size = 64×64, FOV = 22 cm). Thirty oblique axial slices were obtained parallel to the AC-PC with 4-mm slice thickness, 0-mm skip. Cardiac and respiratory activity was monitored using the scanner's built-in photoplethysmograph and a pneumatic belt strapped around the upper abdomen, respectively. Eyes-closed resting-state data were acquired for 11.76 min (1 subject) and 12.24 min (2 subjects). EEG data were acquired during fMRI with a 256-channel system (HCGSN v.1.0 cap and GES 300 amplifier; Electrical Geodesics, Inc., Eugene, OR). The reference was taken as Cz, and data were sampled at 250 Hz using EGI's NetStation 4.5.1 software. The EGI system clock was synchronized with the MRI scanner's 10 MHz master synthesizer, and the scanner also delivered a TTL trigger signal that marked the onset time of every fMRI volume acquisition. In addition, the scanner's photoplethysmograph (PPG) was placed on a finger of the subject's left hand and, with a custom program, used to derive a cardiac QRS marker that was also recorded by the EEG system. The fMRI acquisition was continuous and had uniform spacing between slice excitations. Gradient and ballistocardiogram artifacts in the EEG data were treated using EGI's NetStation software, which implements methods based on template subtraction (Allen et al., 2000) and principal component analysis (Niazy et al., 2005), respectively.

NIH dataset

Magnetic resonance imaging was performed on a 3T whole-body scanner (GE Signa, GE Healthcare Systems, Milwaukee, WI) with a 16-channel receive-only coil array (Nova Medical, Wakefield, MA, USA). Functional images were acquired with a gradient-echo EPI sequence (SENSE factor = 2, TR = 1500 ms, TE = 30 ms, flip angle = 90°, matrix size = 64×48, FOV = 220×165 mm^2). Thirty axial slices were obtained 4-mm thickness, 0-mm skip. Note that the voxel size is identical to that of the Stanford dataset. Cardiac and respiratory activity was monitored using the scanner's built-in photoplethysmograph and a pneumatic belt strapped around the upper abdomen, respectively. For each subject, 390 volumes (9.75 min) of eyes-closed resting-state data were gathered. EEG data were acquired simultaneously with a 31-channel system (international 10–20 montage, one unipolar ECG, 16-bit BrainAmp MR, BrainProducts GmbH, Germany) referenced to FCz and continuously sampled at 5 kHz with a resolution of 0.5 μV/bit and an analog bandwidth from 0.1 to 250 Hz. The EEG sampling clock was synchronized with an external reference signal obtained from the 10 MHz master clock of the MRI scanner. A slice-trigger signal that marked the onset time of every fMRI slice acquisition was also recorded based on a 5 V TTL signal from the scanner, and the fMRI acquisition was evenly spaced with equal delay between each slice excitation. Gradient and ballistocardiogram artifacts in the EEG were reduced using the procedures described in (Liu et al., 2012).

fMRI pre-processing

The fMRI data from both sites were pre-processed identically. The first 4 volumes were discarded to permit stabilization of signal amplitude variation associated with T1 relaxation. Cyclic physiological noise was reduced using RETROICOR with 2nd-order Fourier series on a slice-specific basis (Glover et al., 2000). Slice-timing and motion coregistration (MCFLIRT (Jenkinson et al., 2002)) were performed with FSL (http://www.fmrib.ox.ac.uk/fsl/), and the following nuisance variables were subsequently regressed out of the data: linear and quadratic trends; low-frequency respiratory volume and heart rate, convolved with respiration and cardiac response functions, respectively,

using methods described in (Chang and Glover, 2009); 6 affine motion parameters; and the time series of ROIs in the white matter and cerebrospinal fluid, which were 3 mm-radius spheres centered at MNI coordinates (26, −12, 35) and (19, −33, 18) (identical to those used in (Chang and Glover, 2009)) that were reverse-normalized to native space using SPM (http://www.fil.ion.ucl.ac.uk/spm)). Global signal removal was not performed (Murphy et al., 2009; Saad et al., 2012). Functional images were then normalized to MNI space and smoothed with a 6-mm FWHM Gaussian kernel using SPM.

EEG spectral power

A multitaper time-frequency analysis, implemented with the Chronux toolbox (http://chronux.org; (Mitra and Bokil, 2008)), was performed on the signal from each EEG channel using a moving window of 2 s (overlap = 50%, time-bandwidth product = 3, tapers = 5), yielding a spectrogram for each electrode. The alpha frequency band was defined as a 2 Hz interval centered at each subject's individual peak alpha frequency, which was calculated using the center-of-gravity in frequency approach (Jann et al., 2010; Klimesch et al., 1993), and the alpha power time series at a given electrode was calculated by averaging over this frequency range at each time point in the spectrogram. Theta power was taken across the 4–7 Hz range, and a theta power time series at a given electrode was derived in a similar fashion. The median alpha and theta power time series were then computed over the following 12 electrodes: O1, O2, Oz, P3, P4, Pz, C3, C4, F3, Fz, F4, F7. These particular electrodes were selected because they had corresponding channels in both EEG caps and had not been discarded as noisy in any of the subjects.

Functional networks

Networks for the fMRI analysis were defined using a published atlas of functional ROIs that had been defined from a group-level independent component analysis of resting-state fMRI (Shirer et al., 2012) (http://findlab.stanford.edu/functional_ROIs.html). Functional ROIs were selected as nodes of the default-mode, dorsal attention, and salience networks for the present analysis (Fig. 1, Table 2). The DMN was composed of nodes drawn from the "dorsal DMN", "ventral DMN", and "Precuneus" subnetworks of the atlas, excluding five nodes that fell in areas not typically associated with DMN (thalamus, mid cingulate, and cerebellum). The DAN was composed of all nodes from the network labeled "Visuospatial", and the SN was composed of nodes drawn from the "anterior Salience" and "posterior Salience" networks (excluding those in the cerebellum). The time series of each node was obtained by averaging the time series of its constituent voxels.

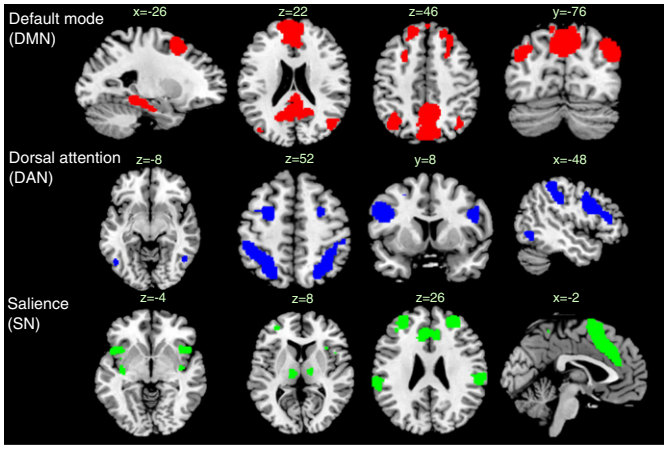

Fig. 1. Networks used in the fMRI connectivity analysis, superimposed on the ch2bet template. Coordinates and node labels are provided in Table 2.

Atlas-defined networks were used in the analysis since we aimed to study fluctuations in functional connectivity both within and between networks, and wished to fix the spatial definition of the nodes beforehand rather than allowing them to be influenced by the correlation structure of the data itself. Yet, the results of atlas-defined networks are meaningful to the extent that they indeed correspond to regions of high functional connectivity in the dataset; this was confirmed by examining the spatial overlap between the atlas-defined networks and a group-level seed based connectivity analysis from one selected node of each network (Supplementary Fig. 1).

Relationship between EEG spectral power and time-varying BOLD functional connectivity

Temporal changes of within- and between-network connectivity were assessed for each resting-state scan on a sliding-window basis (window length = 40 s, with 50% overlap between consecutive windows in order to reduce temporal autocorrelation, as we subsequently apply a linear regression model, described below). For each sliding window, a single metric of functional connectivity between networks *i* and *j* was determined by taking the pairwise correlation coefficient between each node of network *i* and each node of network *j*, applying a Fisher z transform to the correlation coefficient, and averaging the resulting values. For the EEG data, the mean power in the spectral bands of interest was computed in identical sliding windows over the indicated sets of electrodes. In order to account for the approximate hemodynamic delay, a temporal offset of 5 s was applied in calculating the sliding-window power for the EEG data (i.e., the EEG power at time interval $[t-5,\ t-5+W]$ was aligned with the fMRI data at window $[t,\ t+W]$). However, we note that due to the long sliding-window size (40 s), the 5-s offset in fact had a negligible impact on the final results. The reason for simply shifting the time window for EEG calculations, rather than convolving the EEG waveforms with a hemodynamic response function, is because here we are treating EEG power as a state variable in the sliding-window analysis and hence desire the undistorted EEG amplitude values. The rationale for averaging the pairwise correlations between network nodes in order to form a functional connectivity index, rather the alternative approach of first reducing each network to a single time series (via averaging across nodes) and correlating the resulting network signals, is to accommodate potential heterogeneity across network nodes that could be obscured when reducing each network to a single time series. Furthermore, the shared temporal variance amongst network nodes may not necessarily align with the variance shared between each node and the EEG signals.

Statistics were performed using a two-stage hierarchical approach, implemented using functions in *R* (www.r-project.org/). At the individual subject level, the two sliding-window EEG power signals (alpha and theta) were standardized to zero mean and unit variance, and entered into a multiple regression against the sliding-window functional connectivity of each network pair. Regression coefficients were estimated using generalized least squares with an AR1 model for temporal autocorrelation. The resulting coefficient (beta) estimates for each subject were entered into a second-level regression, covarying for the effect of site (NIH or Stanford). Significance was assessed at $p<0.05$ with a Bonferroni correction for multiple comparisons (6 network pairs × 2 bands = 12 comparisons). To subsequently gauge the sensitivity of the results to the sliding window size, the analysis was repeated for window lengths ranging from 20 to 80 s in increments of 5 s, with 50% overlap between successive windows in all cases.

BOLD signal correlations with EEG power fluctuations

An analysis of the correlation between BOLD signal and EEG band power across all time points in the scan was also performed. EEG covariates were obtained by convolving the alpha and theta waveforms (extracted as described above) with the default gamma-variate HRF

Table 2
Composition of functional networks.

Network	Sub-network abbreviation	Number	FIND Atlas node labels	Node centroid (mm) x	y	z
DMN	DMN PCC/ Precuneus	1	Dorsal DMN 04	0.7	−53.2	28.2
		2	Ventral DMN 01	−12.1	−57.8	15.3
		3	Ventral DMN 05	13.1	−53.4	14.3
		4	Ventral DMN 06	0.9	−57.2	54.0
		5	Precuneus 02	2.9	−71.6	39.6
	DMN angular	6	Dorsal DMN 02	−47.6	−67.9	34.6
		7	Dorsal DMN 06	49.9	−63.5	32.1
		8	Precuneus 03	−36.2	−62.3	46.1
		9	Precuneus 04	38.8	−62.0	45.4
	DMN occipital	10	Ventral DMN 04	−36.1	−81.4	32.2
		11	Ventral DMN 09	43.2	−74.4	31.7
	DMN pHG	12	Dorsal DMN 08	−23.5	−28.5	−12.8
		13	Dorsal DMN 09	26.8	−22.6	−17.1
	DMN pHG/ Fusiform	14	Ventral DMN 03	−28.3	−37.1	−15.1
		15	Ventral DMN 08	28.4	−33.5	−19.3
	DMN anterior	16	Dorsal DMN 01	−3.2	49.4	13.7
		17	Dorsal DMN 03	19.3	38.3	47.4
		18	Ventral DMN 02	−24.3	11.7	54.9
		19	Ventral DMN 07	25.6	26.5	45.0
DAN	DAN FEF	20	Visuospatial 01	−26.7	−1.0	54.0
		21	Visuospatial 05	27.9	1.6	54.3
	DAN DLPFC	22	Visuospatial 03	−47.5	13.1	26.7
		23	Visuospatial 07	48.9	11.6	27.9
	DAN IPS	24	Visuospatial 02	−35.8	−46.3	46.9
		25	Visuospatial 06	37.2	−46.8	48.1
	DAN MT	26	Visuospatial 04	−48.6	−64.8	−5.9
		27	Visuospatial 08	50.0	−58.6	−10.7
SN	SN ACC	28	Anterior Salience 03	0.2	17.3	46.9
	SN aPFC	29	Anterior Salience 01	−31.4	46.7	22.2
		30	Anterior Salience 04	28.4	46.0	26.4
	SN aIns	31	Anterior Salience 02	−41.6	14.2	−3.1
		32	Anterior Salience 05	42.6	15.1	−1.4
	SN pIns	33	Posterior Salience 09	−36.6	−13.3	−5.5
		34	Posterior Salience 12	40.3	−6.4	−8.6
	SN SMG	35	Posterior Salience 02	−57.4	−37.7	37.3
		36	Posterior Salience 06	59.2	−32.2	36.4
	SN Thal	37	Posterior Salience 07	−12.4	−21.4	5.2
		38	Posterior Salience 10	12.6	−14.4	8.98

from the SPM software, and these were each entered into separate regression analyses against the whole-brain fMRI data. The fMRI time series at each voxel were scaled to units of percent signal change prior to the regression analysis. The resulting coefficient (beta) maps were entered into a group-level random effects analysis in SPM, covarying for the effect of site (NIH or Stanford).

Results

Relationship between EEG and time-varying fMRI connectivity

The alpha power term in the multiple regression was inversely related to the functional connectivity between DMN and DAN ($t(8) = -8.98$, $p = 0.0002$ Bonferroni-corrected for 12 terms in the multiple regression), while the theta term did not account for functional connectivity between any of the network pairs investigated ($p > 0.05$ Bonferroni-corrected). This is illustrated in Fig. 2. Plots of the sliding-window DMN-DAN connectivity against the alpha term are shown for each individual subject in Fig. 3.

For purposes of comparison, marginal regressions were subsequently performed (i.e. linear regression analyses of DMN-DAN connectivity against the alpha and theta signals separately), as well as regression of a single term consisting of the *ratio* of theta and alpha power. The marginal relationship between DMN-DAN connectivity and alpha power yielded $t(8) = -4.01$, $p = 0.004$, and marginal regression for theta power yielded $t(8) = 0.96$, $p = 0.36$. Using the *ratio* between theta and alpha power yielded $t(8) = 4.62$ $p = 0.002$. (For these three post-hoc marginal regressions, the reported p-values are uncorrected.)

To examine whether the relationship between EEG power and DMN-DAN connectivity is critically dependent on the choice of window size, the analysis was repeated for window sizes ranging from 20 to 80 s (fixing overlap = 50% for all sizes). The alpha term remains significant at the $p < 0.05$-corrected level for window sizes between 30 and 55 s (values ranging from $p = 0.0002$ corrected to $p = 0.022$ corrected), and theta reached significance only at window sizes of 65 and 70 s.

Since the DMN, DAN, and SN as defined here each comprise multiple nodes with heterogeneous functional and anatomic properties, it is of interest to understand the differential contributions of their various sub-networks to the observed effect. Therefore, we next subdivided the networks more finely (Table 2) and performed an identical multiple regression analysis within and between each sub-network. Fig. 4 depicts, for each sub-network pair, the group-level *t* statistic of the alpha and theta regression coefficients; as overall qualitative patterns were of interest, statistical testing was not performed on individual entries. Considering the pattern as a whole, it is apparent that while there is predominantly an inverse relationship between functional connectivity and alpha, the thalamus exhibited *increased* functional connectivity with several nodes as a function of alpha power, particularly with the IPS nodes of the DAN and with other regions of the SN, most strongly the anterior insula. The strongest inverse relationships occurred between the anterior DMN and the MT and FEF regions of the DAN, between the parahippocampal/fusiform and superior occipital regions of the DMN, and between the anterior DMN and the thalamic region of the SN. Consistent with Figs. 2 and 3, increased theta power was associated with increased functional connectivity between nodes of the DMN, particularly within anterior regions. Coupling between area MT and the supramarginal gyrus had the strongest (positive) relationship with theta power amongst the present set of nodes.

EEG alpha and theta power relate to transient anti-correlations between DMN and DAN

Fig. 3 indicates that for most subjects and sliding windows, the sign of the mean node-to-node functional connectivity between the DMN and DAN is positive. However, upon a more detailed inspection of sliding-window correlations on a voxel-wise basis, negative correlations can be observed between various subsets of voxels even during windows whose averaged node-to-node correlations are positive. Therefore, we also examined how the spatial extent of negative correlation between the DMN and DAN on a sliding window basis is related to EEG power. At each sliding window (length = 40 s, 50% overlap), a correlation matrix was computed between the union of all individual voxels comprising the DMN and those comprising the DAN, and the percentage of negative correlation coefficients in the matrix was taken as a metric of anti-correlation spatial extent. The resulting sliding-window time series of DMN-DAN anti-correlation extent was then regressed simultaneously against the EEG alpha and theta bands in the same manner as described above. It was found that alpha power was a significant predictor of increased anti-correlation between DMN-DAN ($t = 3.61$, $p = 0.014$ Bonferroni-corrected for 2 comparisons), while theta

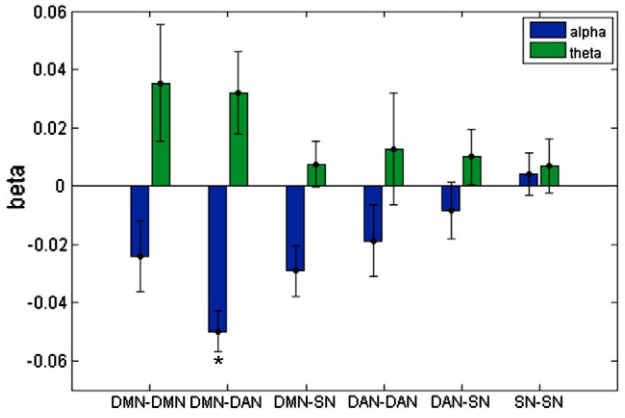

Fig. 2. Beta weights (mean ± standard error across subjects, N = 10) of the multiple regression of standardized EEG alpha and theta power against temporal changes in functional connectivity between nodes of the default mode (DMN), dorsal attention (DAN), and salience networks (SN). Only the relationship between alpha power and DMN-DAN connectivity was significant at a Bonferroni-corrected level of $p<0.05$. Sliding window size = 40 s, overlap 50%.

power was inversely (but not significantly) related ($t = -2.20$, $p = 0.12$, n.s.). An illustration of this phenomenon for one subject (Subject 5) is shown in Fig. 5. Here, for ease of anatomic visualization, we show results of a sliding-window correlation analysis seeded from the mean time series of one node in the DMN (dorsal DMN 04, in the posterior cingulate cortex; see Table 2). Correlations were computed only for voxels contained in the DMN and DAN, and transformed to Fisher z scores. Diminished positive correlations and increased negative correlations were observed in windows with fractionally increased alpha power and lower theta power; increased positive correlations were observed in windows of higher relative theta power and lower relative alpha power.

Relationship between EEG power and fluctuations in BOLD signal variance / local homogeneity

Time-varying fluctuations in BOLD signal variance and local (within-node) homogeneity were also analyzed in order to supplement the above results, as both quantities contribute to the correlation coefficients on which our estimates of cross-network functional connectivity

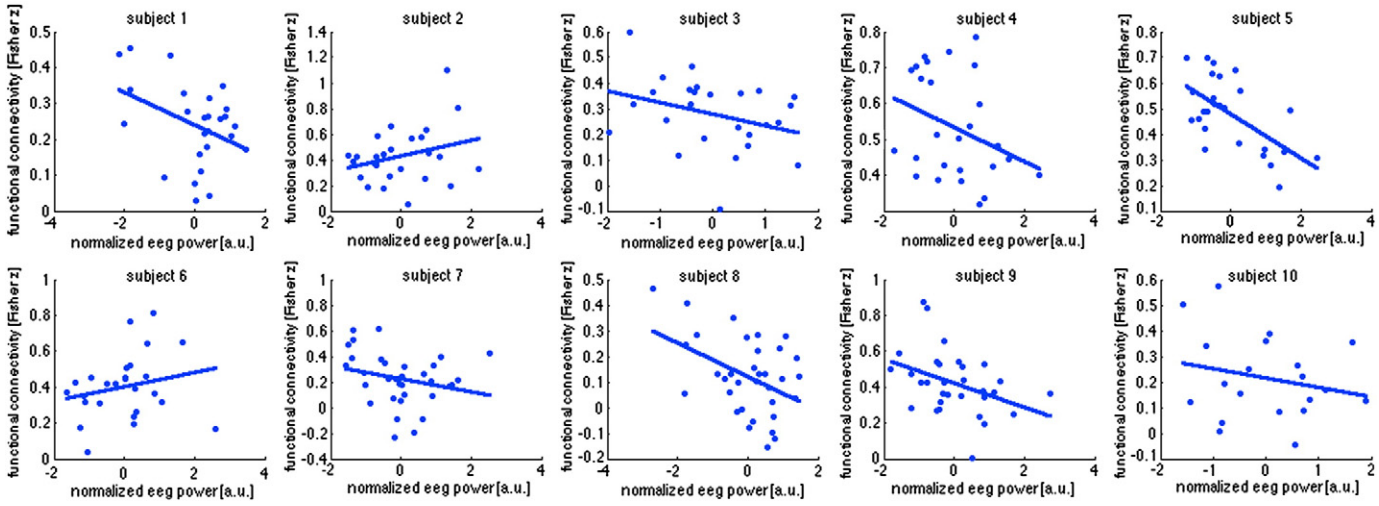

Fig. 3. Marginal relationship between sliding-window EEG alpha band power and the sliding-window measure of functional connectivity between default mode and dorsal attention networks (window size = 40 s, overlap 50%), shown for each subject.

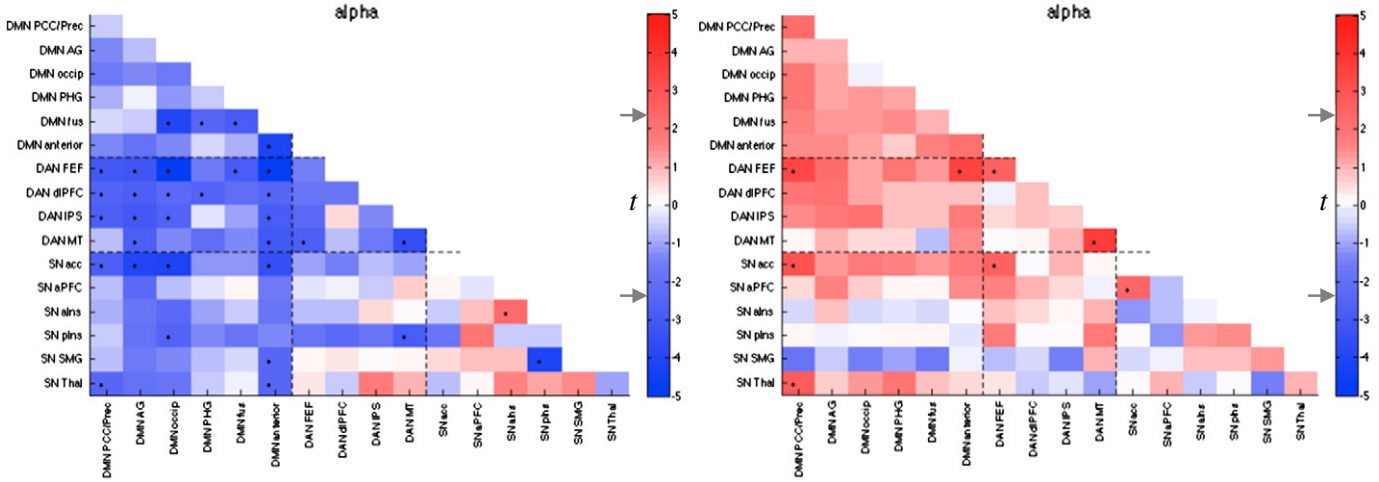

Fig. 4. Relationship between time-varying EEG power and functional connectivity within and between sub-networks (Table 2) of the DMN, DAN, and SN. Color represents the group-level t-score obtained by regressing sliding-window functional connectivity of sub-network pairs against sliding-window EEG alpha and theta power time series. Since this is an exploratory analysis intended to reveal the overall topographic pattern of the previously established effects, only uncorrected t-values are reported. The t-value corresponding to a 2-sided $p = 0.05$ uncorrected ($|t(8)| = 2.3$) is indicated on the colorbar (gray arrows), and suprathreshold entries are indicated in the matrix by '•'.

are based. At each sliding window, (1) the BOLD signal variance was calculated for each individual voxel within the DMN, DAN, and SN; (2) these values were averaged amongst voxels corresponding to the same node, for each of the 38 nodes spanning the three networks (Table 2). By performing the variance analysis for individual voxels prior to averaging within a node, rather than the other way around, we avoid obtaining apparent changes in variance that stem instead from changes in the heterogeneity of voxels within a node. Each node's sliding-window time series of BOLD signal variance was then correlated with the sliding-window EEG alpha power, and repeated for theta power. Fig. 6 (left) shows the mean (±standard error, N = 10) of the correlation coefficients across subjects. A similar analysis was carried out for the local (within-node) homogeneity, which was defined (for each sliding window) as the mean voxel-to-voxel correlation within a given node; results are shown in Fig. 6 (right). Qualitatively, the majority of nodes display an inverse relationship between alpha power and both BOLD signal variance and within-node homogeneity, with the opposite sign for theta. To examine whether the relationship between alpha power and BOLD signal variance (or node homogeneity) was statistically different from that of theta power, paired two-sided t-tests were performed for each network after first averaging, within each subject, the Fisher z-scored correlation between EEG alpha power and variance (or node homogeneity) across the network's constituent nodes. The relationship between alpha power and variance was significantly lower than the correlation between theta power and variance for all 3 networks (DMN: $t(9) = 3.45$, $p = 0.021$; DAN: $t(9) = 3.68$, $p = 0.015$; SN: $t(9) = 2.95$, $p = 0.048$, with p-values reflecting Bonferroni correction for 3 networks). The relationship between alpha power and node homogeneity was *not* significantly lower than the correlation between theta power and variance at a corrected level for any network ($p > 0.05$ Bonferroni).

Stationary correlations between EEG power and BOLD signal time series

A traditional correlation analysis was performed between the posterior alpha and frontal theta power waveforms (convolved with a canonical HRF) and the BOLD signal using all time points in the scan. Group-level statistical maps are depicted in Supplementary Fig. 2. Consistent with a number of previous studies, alpha power showed negative correlations with regions in the occipital cortex (Goldman et al., 2002; Moosmann et al., 2003) as well as prefrontal and parietal attention regions (Laufs et al., 2003). As the threshold was lowered for exploratory purposes, positive correlations in the thalamus, anterior cingulate, and mid cingulate emerged at the highest threshold, also consistent with previous reports (Goldman et al., 2002; Sadaghiani et al., 2010). Theta power showed positive correlations with cuneus/precuneus, superior medial frontal cortex, cerebellar vermis, left mid temporal cortex, and right supramarginal gyrus ($p < 0.05$ corrected).

Finally, we investigated whether the degree to which alpha power was predictive of DMN-DAN functional connectivity may relate to the strength with which the alpha power (convolved with HRF) was negatively correlated with BOLD signal time series in the DAN. For each subject, a measure of the latter was computed by averaging, across all voxels in the DAN, the Fisher-transformed correlation coefficient with the HRF-convolved alpha power time series (where correlation coefficient was computed using all time points in the scan, rather than on a sliding window basis). The resulting measure was then regressed against the subjects' effect size (beta) of the sliding window analysis of alpha power with DMN-DAN connectivity, covarying for scan site. The relationship was in fact negative, with stronger negative correlation between alpha and BOLD signal predicting a *weaker* relationship between alpha and DMN-DAN connectivity ($t = -2.56$, $p = 0.04$), suggesting that the predictive power of alpha-band

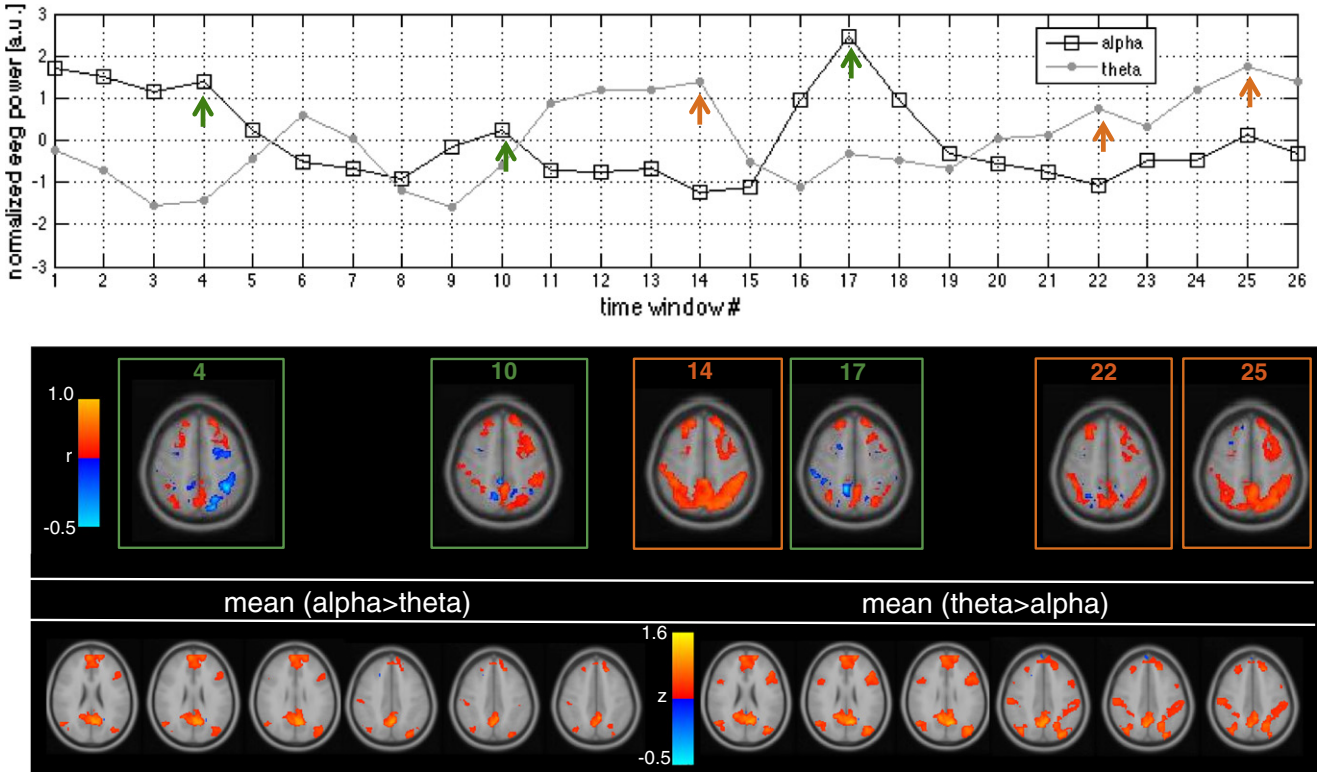

Fig. 5. Relationship between functional connectivity and EEG power in one subject (Subject 5). Top: Time series of temporally normalized sliding-window alpha and theta power, window size = 40 s. Arrows indicate windows selected for visualization of seed-based correlations in the middle panel. Middle: Seed-based correlation maps at the indicated windows. The seed was a single node in the DMN (posterior cingulate cortex), and correlations were computed for each voxel in the DMN and DAN. Bottom: Seed-based functional connectivity maps averaged over all time windows for which normalized alpha power exceeded normalized theta power (bottom left), and vice versa (bottom right). Color represents Fisher z score.

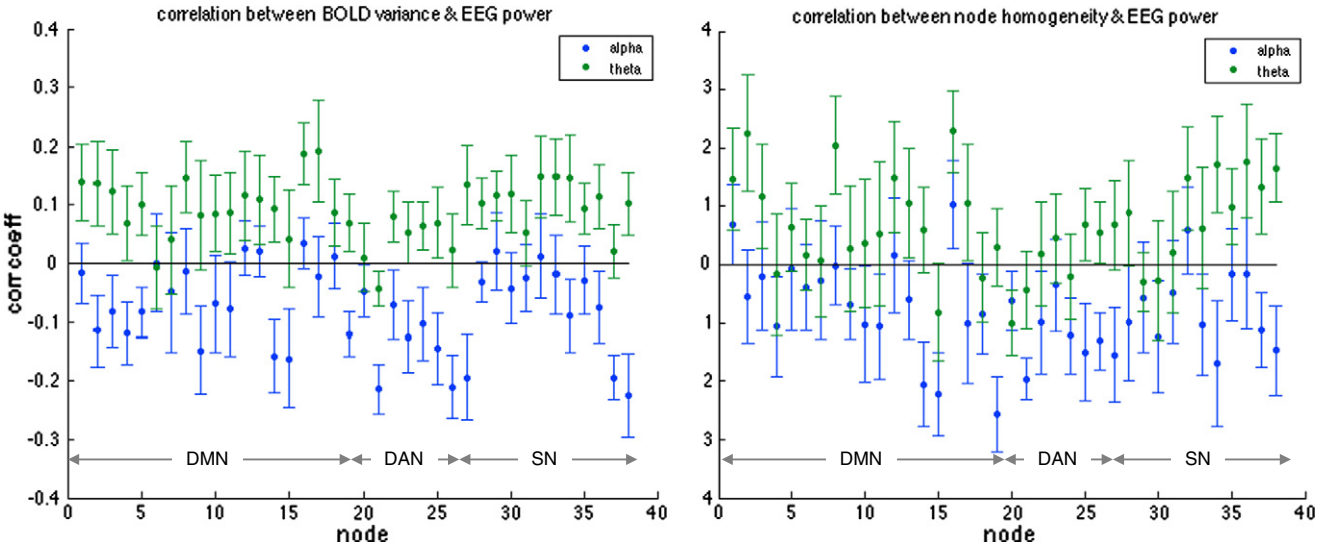

Fig. 6. Relationship between EEG power and time-varying changes in (left) BOLD signal variance and (right) within-node homogeneity. Plots show the mean (±standard error, N = 10) of correlation coefficients across subjects, and data were obtained using a window size of 40 s. Ordering of nodes is consistent with Table 2.

oscillations for DMN-DAN connectivity may not be simply related to BOLD signal correlation or signal-to-noise ratio, though such a phenomenon is difficult to rule out conclusively.

Discussion

The present study provides evidence for electrophysiological signatures of the time-varying connectivity between two large-scale brain networks, the default-mode and dorsal attention systems. Fluctuations in alpha power across time were inversely related to fluctuations in connectivity between DMN and DAN; specifically, epochs of increased alpha power coincided with decreases in positive correlation, as well as increases in the anti-correlation extent, between the DMN and DAN. Results suggest that a significant fraction of resting state connectivity fluctuations may have a neural basis and perhaps reflect state-dependent variations.

Interpretations

The observed relationship between EEG power and DMN-DAN connectivity may arise in part from fluctuating states of arousal and vigilance. Previous studies have linked states of diminished vigilance with relative decreases in alpha power, with corresponding increases in theta and lower frequencies (Klimesch, 1999). Here, we observe that relative decreases in alpha and increases in theta over time were associated with relative increases in the functional connectivity between the DMN and DAN, with similar trends for all other network pairs considered (Fig. 3). These results are consistent with a recent study of moderate sedation with propofol (a state accompanied by EEG signatures similar to that of light sleep), in which increased functional connectivity was observed between the DMN (posterior cingulate seed) and "task positive" regions; i.e., under sedation, the DMN became positively correlated with a network that is typically anti-correlated during wakefulness (Stamatakis et al., 2010). Similarly, the spatial extent of DAN connectivity was found to increase in light sleep compared to wakefulness (Larson-Prior et al., 2011), and the strength of connections within multiple ICA-defined networks grew stronger and more consistent in the progression from wakefulness to light sleep (Fukunaga et al., 2006). Yet, a weakening of functional connectivity between particular regions has also been observed in conditions of low vigilance (e.g. (Greicius et al., 2008; Horovitz et al., 2009)). Our results ought be taken in the context of these varying results, and with consideration of the extent to which findings from sleep and anesthesia generalize to more mild fluctuations in vigilance state during a wakeful resting state.

States of higher vigilance have previously been linked with increased anticorrelation between DMN and DAN. More frequent episodes of anticorrelation in gamma-band local field potentials was reported to occur during waking and REM sleep compared to slow-wave sleep in felines (Popa et al., 2009); human studies report stronger anticorrelation during wake compared to sleep (Horovitz et al., 2009; Samann et al., 2011) and propofol sedation (Boveroux et al., 2010), and in the present study we obtained stronger anticorrelations between DMN and DAN in awake resting states of high alpha power relative to low. Our observation of increased BOLD signal *variance* during higher theta and lower alpha power (Fig. 6) is also consistent with previous reports describing pronounced increases in BOLD signal variance as subjects became progressively drowsy (Fukunaga et al., 2006; Horovitz et al., 2008; Larson-Prior et al., 2011), further suggesting that fluctuations in arousal may mediate the effects seen in our data.

Another potential interpretation relates to varying levels of awareness and mind-wandering in the waking state. Elevated power in the alpha band has been suggested to correspond to a state of alertness and undirected readiness, distinct from focused attention, that may facilitate faster and more accurate task performance (Sadaghiani et al., 2010). Notably, *positive* correlation between DMN and DAN regions has been described during periods of mind wandering, especially in the absence of meta-awareness (Christoff et al., 2009), and because lapses in awareness relate inversely to perceptual readiness (Smallwood et al., 2004), this observation—taken together with the postulated role of alpha in tonic alertness—is consistent with our finding of increased positive correlations between DMN-DAN during epochs of lower alpha power. Moreover, it is in accordance with the observation that increased anticorrelation between DMN-DAN covaries with improved task performance at both the inter- and intra-individual level (Kelly et al., 2008; Thompson et al., 2012). As our resting-state data are limited by the lack of behavioral measure, this interpretation is speculative.

Our findings may also be considered in the context of salience and network switching. Alpha power has been shown to have the strongest positive correlations with regions comprising the salience network (Goldman et al., 2002; Sadaghiani et al., 2010). Here, too, the strongest positive correlations with alpha power were observed in the thalamus

and dorsal anterior cingulate cortex (dACC). The salience network, whose signature nodes include the dACC, anterior insula, and thalamus, has been proposed to influence the activity in the DMN and DAN in both task conditions and resting state (Hamilton et al., 2011; Menon and Uddin, 2010) acting as a "switch" between the respective endogenous and exogenous functions of these networks. Increased alpha (and increased activity in the salience network) may thus correspond to epochs of more frequent switching, consistent with the increases in anticorrelations observed here. Interestingly, while the coupling across most cortical regions decreased as a function of alpha, the average connectivity between the thalamus ROI of the salience network (which appears to lie in primarily in the mediodorsal nucleus) and the anterior insula and several other regions of the salience network tended to increase, supporting the association between spontaneous alpha fluctuations and salience network activity. However, these findings must be interpreted with caution, as (1) they resulted from an un-corrected statistical threshold, and may therefore represent isolated false positives, and (2) the precision of the atlas regions in aligning with the subcortical structure of individual subjects may be low. Careful examination of electrophysiological correlates of subcortical-cortical connectivity may be a worthwhile avenue for future study.

A recent study (Scheeringa et al., 2012) demonstrated, using a psycho-physiological interactions analysis, that dynamic increases in alpha power were linked with decreases in the magnitude of functional connectivity seeded from the visual cortex, both locally (occipital cortex) as well long range (thalamus and ventromedial prefrontal cortex). Findings were postulated to reflect inhibition of functional relationships during higher alpha activity. Our study extends their findings; using a different method of analysis and examining different brain networks (DMN-DAN), we provide further evidence that temporal changes in functional connectivity possesses an EEG correlate, and demonstrate that the effects extend beyond systems directly implicated in alpha rhythm generation.

Limitations and future directions

Several factors may be considered when interpreting our results. First, the peak alpha frequency itself may shift over time (Jann et al., 2010), and it has been shown that an increase in drowsiness is associated with a slowing of the alpha frequency and a shift toward a more anterior distribution (Cantero et al., 2002). Therefore, it is possible that the occurrence of alpha slowing and anteriorization overlaps somewhat with our measure of theta band power. Future work may consider how spatial patterns of alpha and theta power, not simply the power averaged over several electrodes, are altered over time and covary with changes in BOLD functional connectivity. Secondly, a recent study demonstrated that EEG alpha power correlated, in some sessions, with the time course of respiratory variations (Yuan et al., 2012), the latter of which relates to the concentration of arterial CO2 and, consequently, brain perfusion (Birn et al., 2006; Wise et al., 2004). While EEG measurements are believed to be insensitive to hemodynamic artifacts, it is possible that common state changes (e.g. relaxation) mediate both respiration/CO2 concentrations and alpha and/or theta power. Although we attempted to correct for physiological noise during pre-processing, it is possible that residual effects remain.

We did not apply global signal regression (GSR) as a pre-processing step. GSR is known to artificially enhance negative correlations by enforcing a mathematical constraint whereby pairwise correlations sum to zero (Murphy et al., 2009), complicating the interpretation of the data. Regressing out the global average signal likely removes some neural effects of interest, such as contributions from large-scale correlated networks, and the global signal has been shown to correlate with electrophysiological signals in the gamma band as well as lower frequencies (Scholvinck et al., 2010). This is of particular relevance for our study, since we are interested in the dynamics of correlation within and between resting-state networks. It is for these reasons that we had decided not to apply global signal regression, choosing instead to use noise corrections based on concurrent physiological recordings, which have been shown to effectively reduce spatially widespread noise arising from low-frequency respiratory volume and cardiac rate fluctuations (Chang et al., 2009 and Chang and Glover, 2009). By removing a subspace of the global signal derived from physiological models, rather than a whole-brain signal derived from the data itself, we aimed to reduce known sources of noise while leaving intact global fluctuations that are more likely to be of neural origin. We additionally removed signals derived from the white matter and CSF, which presumably carry little (if any) neural fluctuations of interest.

Here, EEG features were linked with BOLD functional connectivity in a sliding-window analysis. The minimum window size in such an analysis is constrained by the time scale at which BOLD functional connectivity evolves, which is considerably slower than that of EEG power variations. Using a time-frequency decomposition of pairwise BOLD coherence, we showed in a previous study that much of the energy of BOLD coherence between nodes of the DMN and DAN is slower than temporal periods of 16 s (Chang and Glover, 2010). Here, while the alpha-FC relationship, as well as the signs of the alpha and theta coefficients, persisted across window sizes ranging from 30 to 55 s, even the smallest window size integrates substantially over power fluctuations in the EEG, thereby potentially ignoring relevant information occurring on faster time scales. Future studies may consider using inverse modeling to characterize the interactions of various fMRI-defined networks at higher temporal resolution, as is being examined for MEG (Brookes et al., 2012; de Pasquale et al., 2010), and may also consider how multiple dynamic features of the EEG within the moving window (beyond simply the average) may relate to BOLD functional connectivity.

For the present analysis, we focused on power in the alpha and theta frequency bands. Beyond having an established relationship with vigilance states (Laufs et al., 2006; Olbrich et al., 2009) and having previously been linked with the BOLD signals in our networks of interest (e.g. (Foster and Parvizi, 2012; Mantini et al., 2007), the choice was guided by noise considerations; there were residual gradient artifact peaks within the beta and gamma bands, the locations of which differed between the Stanford and NIH datasets due to the slightly different acquisition parameters. The delta band was also not considered due to the presence of residual gradient noise around 0 Hz in both of our datasets. Future studies may consider including other frequency bands. Beta band power would be of particular interest in light of findings by Laufs et al., in which two distinct states of alpha-BOLD correlation were identified: (1) a low-alpha, high-theta pattern accompanied by inverse correlations between alpha power and occipital–parietal BOLD activity, posited to reflect drowsiness, and (2) a low-alpha, high-beta pattern accompanied by inverse correlations between alpha power and fronto-parietal BOLD activity, posited to reflect focused attention (Laufs et al., 2006). Distinguishing amongst multiple "alpha states" in the context of BOLD functional connectivity, in addition to activity, may be an interesting future direction. Gamma-band power may also be relevant, as fluctuations in gamma power have been found to correlate with spontaneous BOLD signal activity on spatially widespread scales (Scholvinck et al., 2010; Shmuel and Leopold, 2008). Nir et al. found that correlations in gamma-band local field potential modulations measured with electrocorticography showed a specificity for functional networks (Nir et al., 2008), and—relevant to the concept of alpha states—Magri et al. showed that the relation between alpha and gamma bands is associated with the amplitude of the BOLD signal (Magri et al., 2012).

Also of potential importance are frequencies lower than the theta band, such as in the delta (1–4 Hz) range. Inter-subject variations in delta-band power have been linked with the strength of DMN connectivity (Hlinka et al., 2010). Using invasive electrophysiology in rats, it was found that delta and theta power were predictive of inter-hemispheric

BOLD functional connectivity (Pan et al., 2011) although gamma-band power was most correlated with the local BOLD signal, mirroring our finding that the correlation between alpha power and BOLD signal in the DAN is likely not primarily responsible for the relationship between alpha power and DMN-DAN correlation. Lu et al. reported an association between functional connectivity of bilateral primary somatosensory cortex and correlations in local delta band power fluctuations (measured from epidural EEG) in rats, as both were modulated by anesthetic dose. In a human electrocorticography study, inter-regional correlations in the power fluctuations of the delta band and even lower frequencies (<0.5 Hz) were found to have a spatial structure that aligned with a sensorimotor network defined by resting-state BOLD correlations (He et al., 2008).

Conclusions

The present study contributes to the growing literature on the EEG–fMRI relationship, approaching the question from the perspective of linking band-limited EEG power changes to BOLD functional connectivity. Our data suggest that apparent spontaneous variations in DMN-DAN connectivity possess an electrical signature in the alpha band power, and further suggest that simultaneous measurement of EEG during resting-state scans will provide a greater understanding of variance in functional connectivity and potentially allow one to attribute certain variations to arousal or attentional states.

Supplementary data to this article can be found online at http://dx.doi.org/10.1016/j.neuroimage.2013.01.049.

Acknowledgments

This research was supported by the Intramural Research Program of the National Institute of Neurological Disorders and Stroke, National Institutes of Health. We thank Gary Glover and Qingei Luo for assistance with the Stanford data acquisition, and are grateful to Gang Chen and Ziad Saad for helpful discussion and advice regarding statistics.

References

Allen, P.J., Josephs, O., Turner, R., 2000. A method for removing imaging artifact from continuous EEG recorded during functional MRI. Neuroimage 12, 230–239.
Beckmann, C.F., DeLuca, M., Devlin, J.T., Smith, S.M., 2005. Investigations into resting-state connectivity using independent component analysis. Philos. Trans. R. Soc. Lond. B Biol. Sci. 360, 1001–1013.
Birn, R.M., Diamond, J.B., Smith, M.A., Bandettini, P.A., 2006. Separating respiratory-variation-related fluctuations from neuronal-activity-related fluctuations in fMRI. Neuroimage 31, 1536–1548.
Boveroux, P., Vanhaudenhuyse, A., Bruno, M.A., Noirhomme, Q., Lauwick, S., Luxen, A., Degueldre, C., Plenevaux, A., Schnakers, C., Phillips, C., Brichant, J.F., Bonhomme, V., Maquet, P., Greicius, M.D., Laureys, S., Boly, M., 2010. Breakdown of within- and between-network resting state functional magnetic resonance imaging connectivity during propofol-induced loss of consciousness. Anesthesiology 113, 1038–1053.
Brookes, M.J., Woolrich, M.W., Luckhoo, H., Price, D., Hale, J., Stephenson, M., Barnes, G., Smith, S.M., Morris, P., 2012. The electrophysiological basis of resting state networks. Proc. Int. Soc. Magn. Reson. Med. 20, 132 (Proc. Intl. Soc. Mag. Reson. Med., Melbourne, Australia).
Cantero, J.L., Atienza, M., Salas, R.M., 2002. Human alpha oscillations in wakefulness, drowsiness period, and REM sleep: different electroencephalographic phenomena within the alpha band. Neurophysiol. Clin. 32, 54–71.
Chang, C., Glover, G.H., 2009. Effects of model-based physiological noise correction on default mode network anti-correlations and correlations. Neuroimage 47, 1448–1459.
Chang, C., Cunningham, J.P., Glover, G.H., 2009. Influence of heart rate on the BOLD signal: The cardiac response function. Neuroimage 44, 857–869.
Chang, C., Glover, G.H., 2010. Time-frequency dynamics of resting-state brain connectivity measured with fMRI. Neuroimage 50, 81–98.
Chang, C., Liu, Z., Duyn, J.H., 2012. EEG correlates of non-stationary BOLD functional connectivity. 3rd Bienneial International Conference on Resting State Connectivity, Magdeburg, Germany.
Christoff, K., Gordon, A.M., Smallwood, J., Smith, R., Schooler, J.W., 2009. Experience sampling during fMRI reveals default network and executive system contributions to mind wandering. Proc. Natl. Acad. Sci. U. S. A. 106, 8719–8724.
de Munck, J.C., Goncalves, S.I., Faes, T.J., Kuijer, J.P., Pouwels, P.J., Heethaar, R.M., Lopes da Silva, F.H., 2008. A study of the brain's resting state based on alpha band power, heart rate and fMRI. Neuroimage 42, 112–121.
de Pasquale, F., Della Penna, S., Snyder, A.Z., Lewis, C., Mantini, D., Marzetti, L., Belardinelli, P., Ciancetta, L., Pizzella, V., Romani, G.L., Corbetta, M., 2010. Temporal dynamics of spontaneous MEG activity in brain networks. Proc. Natl. Acad. Sci. U. S. A. 107, 6040–6045.
Foster, B.L., Parvizi, J., 2012. Resting oscillations and cross-frequency coupling in the human posteromedial cortex. Neuroimage 60, 384–391.
Fox, M.D., Snyder, A.Z., Vincent, J.L., Corbetta, M., Van Essen, D.C., Raichle, M.E., 2005. The human brain is intrinsically organized into dynamic, anticorrelated functional networks. Proc. Natl. Acad. Sci. U. S. A. 102, 9673–9678.
Fransson, P., 2005. Spontaneous low-frequency BOLD signal fluctuations: an fMRI investigation of the resting-state default mode of brain function hypothesis. Hum. Brain Mapp. 26, 15–29.
Fukunaga, M., Horovitz, S.G., van Gelderen, P., de Zwart, J.A., Jansma, J.M., Ikonomidou, V.N., Chu, R., Deckers, R.H., Leopold, D.A., Duyn, J.H., 2006. Large-amplitude, spatially correlated fluctuations in BOLD fMRI signals during extended rest and early sleep stages. Magn. Reson. Imaging 24, 979–992.
Glover, G.H., Law, C.S., 2001. Spiral-in/out BOLD fMRI for increased SNR and reduced susceptibility artifacts. Magn. Reson. Med. 46, 515–522.
Glover, G.H., Li, T.Q., Ress, D., 2000. Image-based method for retrospective correction of physiological motion effects in fMRI: RETROICOR. Magn. Reson. Med. 44, 162–167.
Goldman, R.I., Stern, J.M., Engel Jr., J., Cohen, M.S., 2002. Simultaneous EEG and fMRI of the alpha rhythm. Neuroreport 13, 2487–2492.
Greicius, M.D., Krasnow, B., Reiss, A.L., Menon, V., 2003. Functional connectivity in the resting brain: a network analysis of the default mode hypothesis. Proc. Natl. Acad. Sci. U. S. A. 100, 253–258.
Greicius, M.D., Kiviniemi, V., Tervonen, O., Vainionpaa, V., Alahuhta, S., Reiss, A.L., Menon, V., 2008. Persistent default-mode network connectivity during light sedation. Hum Brain Mapp 29, 839–847.
Hamilton, J.P., Furman, D.J., Chang, C., Thomason, M.E., Dennis, E., Gotlib, I.H., 2011. Default-mode and task-positive network activity in major depressive disorder: implications for adaptive and maladaptive rumination. Biol. Psychiatry 70, 327–333.
Handwerker, D.A., Roopchansingh, V., Gonzalez-Castillo, J., Bandettini, P.A., 2012. Periodic changes in fMRI connectivity. Neuroimage 63, 1712–1719.
He, B.J., Snyder, A.Z., Zempel, J.M., Smyth, M.D., Raichle, M.E., 2008. Electrophysiological correlates of the brain's intrinsic large-scale functional architecture. Proc. Natl. Acad. Sci. U. S. A. 105, 16039–16044.
Hlinka, J., Alexakis, C., Diukova, A., Liddle, P.F., Auer, D.P., 2010. Slow EEG pattern predicts reduced intrinsic functional connectivity in the default mode network: an inter-subject analysis. Neuroimage 53, 239–246.
Honey, C.J., Kotter, R., Breakspear, M., Sporns, O., 2007. Network structure of cerebral cortex shapes functional connectivity on multiple time scales. Proc. Natl. Acad. Sci. U. S. A. 104, 10240–10245.
Horovitz, S.G., Fukunaga, M., de Zwart, J.A., van Gelderen, P., Fulton, S.C., Balkin, T.J., Duyn, J.H., 2008. Low frequency BOLD fluctuations during resting wakefulness and light sleep: a simultaneous EEG–fMRI study. Hum. Brain Mapp. 29, 671–682.
Horovitz, S.G., Braun, A.R., Carr, W.S., Picchioni, D., Balkin, T.J., Fukunaga, M., Duyn, J.H., 2009. Decoupling of the brain's default mode network during deep sleep. Proc. Natl. Acad. Sci. U. S. A. 106, 11376–11381.
Hutchison, R.M., Womelsdorf, T., Gati, J.S., Everling, S., Menon, R.S., 2012. Resting-state networks show dynamic functional connectivity in awake humans and anesthetized macaques. Hum. Brain Mapp. (Epub ahead of print).
Jann, K., Koenig, T., Dierks, T., Boesch, C., Federspiel, A., 2010. Association of individual resting state EEG alpha frequency and cerebral blood flow. Neuroimage 51, 365–372.
Jenkinson, M., Bannister, P., Brady, M., Smith, S., 2002. Improved optimization for the robust and accurate linear registration and motion correction of brain images. Neuroimage 17, 825–841.
Kelly, A.M., Uddin, L.Q., Biswal, B.B., Castellanos, F.X., Milham, M.P., 2008. Competition between functional brain networks mediates behavioral variability. Neuroimage 39, 527–537.
Kiviniemi, V., Vire, T., Remes, J., Elseoud, A.A., Starck, T., Tervonen, O., Nikkinen, J., 2011. A sliding time-window ICA reveals spatial variability of the default mode network in time. Brain Connect. 1, 339–347.
Klimesch, W., 1999. EEG alpha and theta oscillations reflect cognitive and memory performance: a review and analysis. Brain Res. Brain Res. Rev. 29, 169–195.
Klimesch, W., Schimke, H., Pfurtscheller, G., 1993. Alpha frequency, cognitive load and memory performance. Brain Topogr. 5, 241–251.
Larson-Prior, L.J., Power, J.D., Vincent, J.L., Nolan, T.S., Coalson, R.S., Zempel, J., Snyder, A.Z., Schlaggar, B.L., Raichle, M.E., Petersen, S.E., 2011. Modulation of the brain's functional network architecture in the transition from wake to sleep. Prog. Brain Res. 193, 277–294.
Laufs, H., 2008. Endogenous brain oscillations and related networks detected by surface EEG-combined fMRI. Hum. Brain Mapp. 29, 762–769.
Laufs, H., Kleinschmidt, A., Beyerle, A., Eger, E., Salek-Haddadi, A., Preibisch, C., Krakow, K., 2003. EEG-correlated fMRI of human alpha activity. Neuroimage 19, 1463–1476.
Laufs, H., Holt, J.L., Elfont, R., Krams, M., Paul, J.S., Krakow, K., Kleinschmidt, A., 2006. Where the BOLD signal goes when alpha EEG leaves. Neuroimage 31, 1408–1418.
Liu, Z., de Zwart, J.A., van Gelderen, P., Kuo, L.W., Duyn, J.H., 2012. Statistical feature extraction for artifact removal from concurrent fMRI-EEG recordings. Neuroimage 59, 2073–2087.
Lu, H., Zuo, Y., Gu, H., Waltz, J.A., Zhan, W., Scholl, C.A., Rea, W., Yang, Y., Stein, E.A., 2007. Synchronized delta oscillations correlate with the resting-state functional MRI signal. Proc. Natl. Acad. Sci. U. S. A. 104, 18265–18269.
Magri, C., Schridde, U., Murayama, Y., Panzeri, S., Logothetis, N.K., 2012. The amplitude and timing of the BOLD signal reflects the relationship between local field potential power at different frequencies. J. Neurosci. 32, 1395–1407.

Makeig, S., Inlow, M., 1993. Lapses in alertness: coherence of fluctuations in performance and EEG spectrum. Electroencephalogr. Clin. Neurophysiol. 86, 23–35.
Mantini, D., Perrucci, M.G., Del Gratta, C., Romani, G.L., Corbetta, M., 2007. Electrophysiological signatures of resting state networks in the human brain. Proc. Natl. Acad. Sci. U. S. A. 104, 13170–13175.
Menon, V., Uddin, L.Q., 2010. Saliency, switching, attention and control: a network model of insula function. Brain Struct. Funct. 214, 655–667.
Mitra, P., Bokil, H., 2008. Observed Brain Dynamics. Oxford University Press, New York.
Moosmann, M., Ritter, P., Krastel, I., Brink, A., Thees, S., Blankenburg, F., Taskin, B., Obrig, H., Villringer, A., 2003. Correlates of alpha rhythm in functional magnetic resonance imaging and near infrared spectroscopy. Neuroimage 20, 145–158.
Murphy, K., Birn, R.M., Handwerker, D.A., Jones, T.B., Bandettini, P.A., 2009. The impact of global signal regression on resting state correlations: are anti-correlated networks introduced? Neuroimage 44, 893–905.
Niazy, R.K., Beckmann, C.F., Iannetti, G.D., Brady, J.M., Smith, S.M., 2005. Removal of FMRI environment artifacts from EEG data using optimal basis sets. Neuroimage 28, 720–737.
Nir, Y., Mukamel, R., Dinstein, I., Privman, E., Harel, M., Fisch, L., Gelbard-Sagiv, H., Kipervasser, S., Andelman, F., Neufeld, M.Y., Kramer, U., Arieli, A., Fried, I., Malach, R., 2008. Interhemispheric correlations of slow spontaneous neuronal fluctuations revealed in human sensory cortex. Nat. Neurosci. 11, 1100–1108.
Olbrich, S., Mulert, C., Karch, S., Trenner, M., Leicht, G., Pogarell, O., Hegerl, U., 2009. EEG-vigilance and BOLD effect during simultaneous EEG/fMRI measurement. Neuroimage 45, 319–332.
Pan, W.J., Thompson, G., Magnuson, M., Majeed, W., Jaeger, D., Keilholz, S., 2011. Broadband local field potentials correlate with spontaneous fluctuations in functional magnetic resonance imaging signals in the rat somatosensory cortex under isoflurane anesthesia. Brain Connect. 1, 119–131.
Petridou, N., Gaudes, C.C., Dryden, I.L., Francis, S.T., Gowland, P.A., 2012. Periods of rest in fMRI contain individual spontaneous events which are related to slowly fluctuating spontaneous activity. Hum. Brain Mapp. (Epub ahead of print).
Popa, D., Popescu, A.T., Pare, D., 2009. Contrasting activity profile of two distributed cortical networks as a function of attentional demands. J. Neurosci. 29, 1191–1201.
Rack-Gomer, A.L., Liu, T.T., 2012. Caffeine increases the temporal variability of resting-state BOLD connectivity in the motor cortex. Neuroimage 59, 2994–3002.
Saad, Z.S., Gotts, S.J., Murphy, K., Chen, G., Jo, H.J., Martin, A., Cox, R.W., 2012. Trouble at rest: how correlation patterns and group differences become distorted after global signal regression. Brain Connect. 2, 25–32.
Sadaghiani, S., Scheeringa, R., Lehongre, K., Morillon, B., Giraud, A.L., Kleinschmidt, A., 2010. Intrinsic connectivity networks, alpha oscillations, and tonic alertness: a simultaneous electroencephalography/functional magnetic resonance imaging study. J. Neurosci. 30, 10243–10250.
Sakoglu, U., Pearlson, G.D., Kiehl, K.A., Wang, Y.M., Michael, A.M., Calhoun, V.D., 2010. A method for evaluating dynamic functional network connectivity and task-modulation: application to schizophrenia. MAGMA 23, 351–366.
Samann, P.G., Wehrle, R., Hoehn, D., Spoormaker, V.I., Peters, H., Tully, C., Holsboer, F., Czisch, M., 2011. Development of the brain's default mode network from wakefulness to slow wave sleep. Cereb. Cortex 21, 2082–2093.
Scheeringa, R., Petersson, K.M., Kleinschmidt, A., Jensen, O., Bastiaansen, M.C., 2012. EEG alpha power modulation of fMRI resting state connectivity. Brain Connect. 2, 254–264.
Scholvinck, M.L., Maier, A., Ye, F.Q., Duyn, J.H., Leopold, D.A., 2010. Neural basis of global resting-state fMRI activity. Proc. Natl. Acad. Sci. U. S. A. 107, 10238–10243.
Shirer, W.R., Ryali, S., Rykhlevskaia, E., Menon, V., Greicius, M.D., 2012. Decoding subject-driven cognitive states with whole-brain connectivity patterns. Cereb. Cortex 22, 158–165.
Shmuel, A., Leopold, D.A., 2008. Neuronal correlates of spontaneous fluctuations in fMRI signals in monkey visual cortex: implications for functional connectivity at rest. Hum. Brain Mapp. 29, 751–761.
Shmueli, K., van Gelderen, P., de Zwart, J.A., Horovitz, S.G., Fukunaga, M., Jansma, J.M., Duyn, J.H., 2007. Low-frequency fluctuations in the cardiac rate as a source of variance in the resting-state fMRI BOLD signal. Neuroimage 38, 306–320.
Smallwood, J., Davies, J.B., Heim, D., Finnigan, F., Sudberry, M., O'Connor, R., Obonsawin, M., 2004. Subjective experience and the attentional lapse: task engagement and disengagement during sustained attention. Conscious. Cogn. 13, 657–690.
Smith, S.M., Fox, P.T., Miller, K.L., Glahn, D.C., Fox, P.M., Mackay, C.E., Filippini, N., Watkins, K.E., Toro, R., Laird, A.R., Beckmann, C.F., 2009. Correspondence of the brain's functional architecture during activation and rest. Proc. Natl. Acad. Sci. U. S. A. 106, 13040–13045.
Sporns, O., 2011. The non-random brain: efficiency, economy, and complex dynamics. Front. Comput. Neurosci. 5, 5.
Stamatakis, E.A., Adapa, R.M., Absalom, A.R., Menon, D.K., 2010. Changes in resting neural connectivity during propofol sedation. PLoS One 5, e14224.
Thompson, G.J., Magnuson, M.E., Merritt, M.D., Schwarb, H., Pan, W.J., McKinley, A., Tripp, L.D., Schumacher, E.H., Keilholz, S.D., 2012. Short-time windows of correlation between large-scale functional brain networks predict vigilance intraindividually and interindividually. Hum. Brain Mapp. (Epub ahead of print).
Uddin, L.Q., Kelly, A.M., Biswal, B.B., Xavier Castellanos, F., Milham, M.P., 2009. Functional connectivity of default mode network components: correlation, anticorrelation, and causality. Hum. Brain Mapp. 30, 625–637.
Vanhaudenhuyse, A., Noirhomme, Q., Tshibanda, L.J., Bruno, M.A., Boveroux, P., Schnakers, C., Soddu, A., Perlbarg, V., Ledoux, D., Brichant, J.F., Moonen, G., Maquet, P., Greicius, M.D., Laureys, S., Boly, M., 2010. Default network connectivity reflects the level of consciousness in non-communicative brain-damaged patients. Brain 133, 161–171.
Wise, R.G., Ide, K., Poulin, M.J., Tracey, I., 2004. Resting fluctuations in arterial carbon dioxide induce significant low frequency variations in BOLD signal. Neuroimage 21, 1652–1664.
Yuan, H., Zotev, V., Phillips, R., Bodurka, J., 2012. Correlated slow fluctuations in respiration, EEG, and BOLD fMRI: what is the origin of physiological noise? Proc. Int. Soc. Magn. Reson. Med. 20, 2843 (Proc. Intl. Soc. Mag. Reson. Med., Melbourne, Australia).